Binocular receptive field models, disparity tuning, and characteristic disparity

Yu-Dong Zhu and Ning Qian

Center for Neurobiology and Behavior
Columbia University
New York, NY 10032

Abbreviated title: Binocular receptive field models and disparity tuning

Send all correspondence to:

Dr. Ning Qian
Center for Neurobiology and Behavior
Columbia University
722 W. 168th Street
New York, NY 10032
(212) 960-2213 (phone)
(212) 960-2561 (fax)
nq6@columbia.edu (email)

Abstract

Disparity tuning of visual cells in the brain depends on the structure of their binocular receptive fields (RFs). Freeman and coworkers have found that binocular RFs of a typical simple cell can be quantitatively described by two Gabor functions with the same Gaussian envelope but different phase parameters in the sinusoidal modulations (Freeman and Ohzawa, 1990). This phase-parameter based RF description, however, has recently been questioned by Wagner and Frost (1993) based on their identification of a so-called characteristic disparity (CD) in some cells' disparity tuning curves. They concluded that their data favor the traditional binocular RF model which assumes an overall positional shift between a cell's left and right RFs. Here we set to resolve this issue by studying the dependence of cells' disparity tuning on their underlying RF structures through mathematical analyses and computer simulations. We model the disparity tuning curves in Wagner and Frost's experiments and demonstrate that the mere existence of approximate CDs in real cells cannot be used to distinguish the phase-parameter based RF description from the traditional position-shift based RF description. Specifically, we found that model simple cells with either type of RF description do not have a CD. Model complex cells with the position-shift based RF description have a precise CD, and those with the phase-parameter based RF description have an approximate CD. We also suggest methods for correctly distinguishing the two types of RF descriptions. A hybrid of the two RF models may be required to fit the behavior of some real cells and we show how to determine the relative contributions of the two RF models.

1 Introduction

Binocular disparity provides the sensory cue for stereoscopic depth perception. It is now well established that many cells in the visual cortex are tuned to binocular disparity and could thus form the neural substrate of stereo vision (Bishop and Pettigrew, 1986; Poggio and Poggio, 1984). However, the exact receptive field (RF) organization responsible for the observed disparity tuning of these cells remains controversial. Early physiological studies suggested that disparity tuning was created by a retinal positional shift between the left and right RFs of a binocular cell (Bishop, Henry and Smith, 1971; Maske, Yamane and Bishop, 1984). The shapes of the two RF profiles of a given cell were usually assumed to be identical. Although such a position-shift based RF description has an intuitive appeal, the main limitation of these early studies is that cells' RFs were usually mapped manually and the results were therefore only qualitative.

Quantitative mapping of binocular RFs was performed relatively recently by Freeman and collaborators (Ohzawa, DeAngelis and Freeman, 1990; DeAngelis, Ohzawa and Freeman, 1991) using the automated reverse correlation technique (Jones and Palmer, 1987). These studies indicate that binocular RFs of a simple cell in the cat primary visual cortex can be well described by two Gabor functions, one for each eye. (A Gabor function is simply a product of a Gaussian envelope and a sinusoid.) It was found that the left and right RFs of a cell often have somewhat different shapes, and that this shape difference can be easily accounted for by letting the two Gabor functions have the same Gaussian envelopes (on the corresponding left and right retinal locations) but different phase parameters in the sinusoids. The phase parameter difference creates a shift between the two sinusoids within their registered Gaussian windows, and this shift generates disparity sensitivity for the cell.

The phase-parameter based RF description of Freeman et al. has recently been questioned by Wagner and Frost (1993) based on their discovery of a so-called characteristic disparity (CD) in some cells recorded from the visual Wulst of the barn owl (see also Pettigrew (1993)). For a given cell Wagner and Frost first obtained its disparity tuning curve using spatial noise stimuli. There is usually a main peak in the tuning curve flanked by smaller side peaks. They then recorded from the same cell with sinusoidal gratings of various spatial frequencies and obtained a family of disparity tuning curves, one for each grating frequency. Each of these grating tuning curves is periodic with a period equal to that of the stimuli. The interesting finding is that for some cells one set of peaks of the grating tuning curves and the main peak of the noise tuning curve tend to align approximately at a certain disparity. They called this disparity the characteristic disparity of the cell (cf. Fig. 8). They concluded that their data are consistent with the traditional position-shift type of RF organization (termed "CD model" in their paper) but not with the phase-parameter type of RF model proposed by Freeman and coworkers.

To resolve this controversy, it is important to note that one cannot predict a cell's disparity tuning curves to a given set of stimuli with only the knowledge of the cell's RF profiles. The other crucial piece of information is a procedure that determines a cell's response as a function of its RF profiles and the visual pattern falling on the RFs. We will call this procedure the response model of a cell. Obviously, a given RF model can be combined with different response models to produce different disparity tuning curves. (For example, one response model might add the contributions from the two RFs of a binocular cell while an-

other might multiply the two RF contributions.) Unfortunately, Wagner and Frost did not specify a response model when stating their conclusion. In addition, they did not model the shapes of the disparity tuning curves they recorded.

We therefore decided to investigate how a cell's disparity tuning to a stimulus depends on its underlying RF model and response model, and to re-examine the implications of Wagner and Frost's CD data. We will show that with a physiologically determined response model for simple cells, neither the position-shift based RF description nor the phase-parameter based RF description has a CD. CDs can only be defined at the level of complex cells. We will suggest methods for correctly distinguishing the two types of RF model. We will also consider the possibility of a hybrid model and demonstrate how to determine the relative contributions of position shifts and phase parameters to the disparity tuning of real cells. Some preliminary results have been reported previously in abstract form (Qian, 1994b).

2 Analyses and Simulations

Since we are only concerned with horizontal disparity, we will use one-dimensional RF profiles in our analyses and simulations. As mentioned above, Freeman and coworkers found that binocular spatial RFs of a typical simple cell can be described by two Gabor functions with the same Gaussian envelopes but different sinusoidal modulations. Mathematically, the left and right RFs of a simple cell centered at $x = 0$ are given by the following equations:

$$f_l(x) = exp(-\frac{x^2}{2\sigma^2})cos(\omega_0 x + \phi_l) \tag{1}$$

$$f_r(x) = exp(-\frac{x^2}{2\sigma^2})cos(\omega_0 x + \phi_r) \tag{2}$$

where σ and ω_0 are the Gaussian width and the preferred (angular) spatial frequency of the RFs; ϕ_l and ϕ_r are the left and right phase parameters. Intuitively, the Gaussian terms in the Gabor functions determine the overall sizes and locations of the RFs and the sinusoidal terms determine the excitatory and inhibitory subregions within the RFs. The difference between the two phase parameters generates a relative displacement between the sinusoidal modulations as well as a shape difference between the two RF profiles (see Fig. 1). We will show that this displacement will be related to the preferred disparity at the level of complex cells.

In contrast, the traditional position-shift type of spatial RF model assumes an overall displacement (for both the envelopes and the modulations) between the left and right RF profiles. Under this model, the two RF profiles of a binocular simple cell can be written as:

$$f_l(x) = exp(-\frac{x^2}{2\sigma^2})cos(\omega_0 x + \phi) \tag{3}$$

$$f_r(x) = f_l(x - d) \equiv exp(-\frac{(x-d)^2}{2\sigma^2})cos(\omega_0 (x - d) + \phi) \tag{4}$$

where σ and ω_0 are again the Gaussian width and the preferred spatial frequency of the RFs. ϕ is a common phase parameter included for generality; it is always the same for the left and right RFs and therefore not related to disparity sensitivity. The two RF profiles have identical shapes but are shifted relative to each other by the distance d. These two different types of RF models are depicted in Fig. 1.

——— Place Fig. 1 about here ———

As we mentioned in the Introduction, in addition to a spatial RF model, we also need a response model in order to calculate a cell's disparity tuning to a stimulus. The most quantitative response models to date for binocular cells also come from physiological studies by Freeman et al.(Freeman and Ohzawa, 1990; Ohzawa et al., 1990; DeAngelis et al., 1991) (see also Ferster (1981) for an earlier study with quantitative modeling). They showed that to a good approximation, a binocular simple cell's response can be determined by first computing the correlation between the spatial RF profile and the visual pattern falling on it for each eye, and then adding the two correlations from the two eyes. They further showed that a binocular complex cell's response can be modeled by summing the squared responses of a quadrature pair of binocular simple cells. We will use these response models in our calculations.

2.1 Disparity tuning of simple cells

We first consider simple cell disparity tuning curves. According to the physiological studies by Freeman et al., the response of a simple cell is given by:

$$r_s = \int_{-\infty}^{+\infty} dx[f_l(x)I_l(x) + f_r(x)I_r(x)] \tag{5}$$

where $f_l(x)$ and $f_r(x)$ are the left and right RF profiles, and $I_l(x)$ and $I_r(x)$ are the left and right retinal images of the stimulus. (For a layer of simple cells with identical properties but different RF locations, Equation 5 should be written as a convolution.) Note that such a linear response model does not take the effect of contrast saturation into account. However, the model is good enough for our purpose since we are mainly interested in the peak locations of disparity tuning curves (see the Discussion). Also note that the temporal dimension of the RFs and stimulus is not included since we have shown elsewhere that it does not affect the disparity tuning of a cell unless an interocular time delay is introduced (Qian and Andersen, 1996).

With Equation 5, the responses of simple cells can be calculated for any given RF profiles and stimuli, either numerically or analytically. The details of our mathematical analysis are given in the Appendix. The main conclusion is that simple cells with either the phase-parameter based RF description or the position-shift based RF description cannot have a CD because their disparity tuning to any stimuli strongly depends on the Fourier phases (i.e., the phases of the Fourier transforms) of the stimuli. Two independently generated spatial noise patterns have different Fourier phases even when they contain the same disparity and have identical overall textural appearance. Consequently, the disparity tuning curves obtained with two sets of independently generated spatial noise patterns will have different

peak locations. This result was confirmed previously through computer simulations for simple cells with the phase-parameter based RF model (Qian, 1994a). Similar simulation results for a simple cell with the position-shift based RF model are shown in Fig. 2. Here the disparity tuning curves of a simple cell to two sets of independently generated random dot patterns are plotted. It is clear from the figure that the peak locations of the two tuning curves from the same simple cell are very different. Likewise, the disparity tuning curves of a simple cell to two sets of sinusoidal gratings of the same frequency but positioned differently with respect to the cell's RFs will also have different peak locations (results not shown). Simple cells therefore do not have well-defined disparity tuning curves (Ohzawa et al., 1990; Qian, 1994a). Since CD is defined according to the peak locations of the noise and grating disparity tuning curves we conclude that simple cells do not have a CD.

——— Place Fig. 2 about here ———

The dependence of simple cell responses to stimulus Fourier phases can be understood intuitively by considering the disparity tuning of a simple cell to a vertical line. The Fourier phase of the line is simply proportional to the position of the line. For a given disparity of the line, the response of the simple cell is not fixed; it also depends on the position (or equivalently, the Fourier phase) of the line in the RFs since the cell has separate excitatory and inhibitory subregions within its RFs. A given disparity of the line may evoke strong response at one line position because it happens to fall on the excitatory subregions of both RFs but may evoke a much weaker response at a different line position because it may now happen to stimulate some inhibitory part(s) of the RFs. Therefore, disparity tuning curves of simple cells to line stimuli are Fourier phase dependent. Similar arguments can be made for the cases with spatial noise patterns and sinusoidal gratings.

2.2 Disparity tuning of complex cells

We now turn to complex cell responses. As we mentioned before, Freeman and coworkers also proposed a response model for complex cells based on their quantitative physiological experiments. They found that the response of a binocular complex cell can be simulated by summing up the squared responses of a quadrature pair of simple cells (Freeman and Ohzawa, 1990; Ohzawa et al., 1990). This quadrature pair method is a binocular generalization of that used previously in motion energy models (Adelson and Bergen, 1985; Watson and Ahumada, 1985), and has also been derived based on theoretical considerations by Qian (1994a). Specifically, two binocular simple cells are said to form a quadrature pair if the sinusoidal modulations of their left and right RFs both have a 90° phase difference while all the other parameters of the two cells are identical. Therefore, for the phase-parameter based RF description two cells form a quadrature pair if their left and right phase parameters in Equations 1 and 2 are related by:

$$\phi_{l,2} = \phi_{l,1} + \pi/2, \tag{6}$$

$$\phi_{r,2} = \phi_{r,1} + \pi/2 \tag{7}$$

where the subscripts 1 and 2 label the parameters of the two cells in the pair. For the position-shift type of RF description described by Equations 3 and 4, there is a common

phase parameter for both the left and right RFs and this parameter is related by:

$$\phi_2 = \phi_1 + \pi/2 \tag{8}$$

for a quadrature pair of simple cells. The response of a complex cell constructed from a single quadrature pair is then calculated according to:

$$r_q = (r_{s,1})^2 + (r_{s,2})^2 \tag{9}$$

where $r_{s,1}$ and $r_{s,2}$ are the responses of the two simple cells in the pair. Note that one can also replace the "+" signs in Equations 6 to 8 by the "−" signs without changing the response of a quadrature pair since such a transformation merely reverses the sign of the simple cell responses (see Equations 1 to 5).

Based on both physiological and computational grounds, we add one final step to the above response model for complex cells: instead of using a single quadrature pair of simple cells to compute the response of a complex cell, we perform a weighted average of several quadrature pairs with nearby and overlapping RFs. All other parameters are identical among these quadrature pairs. Mathematically, the complex cell response is given by:

$$r_c = r_q * w \tag{10}$$

where r_q is the response of a single quadrature pair given by Equation 9, w is a spatial weighting function, and $*$ denotes the convolution operation. This procedure can be viewed as the implementation of the physiological fact that average complex cells have somewhat larger RFs than those of simple cells (Hubel and Wiesel, 1962; Schiller, Finlay and Volman, 1976). (Without this pooling step, a complex cell constructed from a single quadrature pair would have the same RF size as that of the constituent simple cells.) Computationally, this averaging step makes the disparity tuning of the resulting complex cells much more reliable (see the Appendix and Qian and Zhu (1995)). In our simulations, the weighting function w was chosen to be a symmetric two-dimensional (2D) Gaussian. We found that the disparity tuning curves of the complex cells are not very sensitive to the width σ_w of the Gaussian so long as it is larger than 1 pixel. (The sampling artifacts associated with a very narrow Gaussian are not important here because any reasonable weighting function can be used for the pooling step.)

The above equations specify a complete response model for complex cells. We can now calculate the disparity tuning curves of complex cells constructed from simple cells with either the phase-parameter based or the position-shift based RF description. As we show in the Appendix, some general analyses can be made without explicit knowledge of the input stimuli. The analytical results indicate that, unlike simple cells, the responses of complex cells only depend on the Fourier amplitudes of the input stimuli but not on their Fourier phases. This is true for both the phase-parameter and the position-shift based RF descriptions. Therefore, complex cells with either type of RF description do not suffer from the Fourier phase problem, and have well-defined disparity tuning curves. We have performed computer simulations to confirm this conclusion. An example for a complex cell with the position-shift based RF model is shown in Fig. 3. The figure shows the disparity tuning curves of the complex cell to two sets of independently generated spatial noise patterns. Unlike the simple

cell shown in Fig.2, the two tuning curves of the complex cell have very similar shapes and nearly identical peak locations. Similar results (not shown) have been obtained for complex cells with the phase-parameter based RF model.

——— Place Fig. 3 about here ———

The existence of reliable disparity tuning curves is a necessary but not sufficient condition for the existence of CD. We next examine whether model complex cells can have CDs similar to those found in real cells recorded by Wagner and Frost (1993), and how the results depend on the types of RF models.

2.3 Complex cells with position-shift based RF model

We first consider complex cells constructed from simple cells with the position-shift based RF model. Since CDs are defined according to the peak locations of the noise and grating disparity tuning curves, we calculate complex cell responses to these stimuli. It can be shown that the response of a complex cell to a spatial noise pattern with disparity D is given by (see the Appendix):

$$r_{c,noise}^{pos} \approx 16\pi^2\rho^2 exp[-\frac{(D-d)^2}{4\sigma^2}]cos^2[\frac{\omega_0}{2}(D-d)] \tag{11}$$

where ρ denotes the Fourier amplitude of the stimulus (which is a frequency-independent constant for noise patterns). σ, ω_0 and d are the intrinsic parameters of the simple cells used to construct the complex cell. They are the Gaussian width, the preferred spatial frequency and the shift between the left and right RFs of the simple cells. The disparity tuning curve of the complex cell to spatial noise patterns can be obtained by plotting Equation 11 as a function of stimulus disparity D while keeping all other parameters constant. One such plot is shown in Fig. 4 (part a).

According to Equation 11, a complex cell with the position-shift based RF profiles responds optimally when the disparity D of the spatial noise stimulus is equal to the relative displacement d between the two RFs. Therefore, the disparity tuning curve has a main peak at $D = d$. It also has side peaks at $D = d \pm 2\pi n/\omega_0$ where $n = 1, 2, \cdots$. The distance between any two adjacent peaks in the tuning curve is equal to the preferred spatial period of the cell ($2\pi/\omega_0$). The side peaks decay away with increasing difference between the disparity D and the cell's shift parameter d according to the Gaussian term in Equation 11.

——— Place Fig. 4 about here ———

The response of the complex cell to a sine wave grating with spatial frequency Ω is given by (see the Appendix):

$$r_{c,sin}^{pos} = c^2 exp[-\frac{(\Omega-\omega_0)^2\sigma^2}{2}]cos^2[\frac{\Omega}{2}(D-d)] \tag{12}$$

where c is a constant independent of disparity D. A plot of Equation 12 is shown in Fig. 4 (part b). The Gaussian term in the above equation determines the spatial frequency tuning

of the cell; only those gratings with frequencies (Ω's) near the cell's preferred frequency (ω_0) can elicit good responses from the cell. Note that unlike Equation 11, the Gaussian term in Equation 12 is not a function of stimulus disparity D. It therefore only contributes a global scaling factor to the disparity tuning curve. The shape of the disparity tuning curve is determined by the periodic cosine term in Equation 12. (The periodicity of the grating tuning curve is expected because as the disparity between the left and right gratings reaches one full cycle, the two gratings become identical and the disparity falls back to zero.) For a given frequency Ω of the grating, the tuning curve has many evenly spaced peaks of the same height, with the distance between any two adjacent peaks equal to the spatial period of the grating ($2\pi/\Omega$). Tuning curves obtained under different grating frequencies have different spacings between their peaks and, in general, have different peak locations. However, according to Equation 12 there is always a response peak at $D = d$ for all grating frequencies (Ω's). This is also the location of the main peak in the noise tuning curve of the same cell (see Equations 11). We therefore conclude that a complex cell with the position-shift based RF description has a CD equal to the shift parameter d.

To see the above conclusion graphically, we have plotted the normalized disparity tuning curves to spatial noise patterns and to sinusoidal gratings of three different frequencies using the analytical expressions in Equations 11 and 12. The results are shown in Fig. 4. The Gaussian width σ and the preferred spatial frequency ($\omega_0/2\pi$) of the constituent simple cells' binocular RFs are 2° and 0.25 cycles/degree respectively, and the shift parameter d is 1°. As expected, the cell has a CD of 1°, which is marked by the vertical line in the figure.

It should be noted that the above set of parameters was chosen for illustrative purposes. Other sets of parameters work equally well. For example, to model a parafoveal cell with small RFs, we could scale down the above set of parameters by a factor of, say, 10. The resulting complex cell would have RFs with a σ equal to 0.2° and a CD equal to 0.1°. This comment applies to all the analytical and simulated results throughout the paper.

Reasonable approximations were used in deriving the analytical results above (see the Appendix). To check the accuracy of our analyses we have also performed numerical simulations. An example is shown in Fig. 5 where normalized noise and grating disparity tuning curves of a complex cell with the position-shift based RFs are plotted. For the purpose of comparison, we have chosen the parameters in the simulations to be identical to those for plotting the analytical results in Fig. 4. For cells with RF Gaussian width (σ) equal to 2°, four pixels were used in our simulations to represent 1° of visual angle and a total of 65 pixels were used to describe each RF profile. Input stimuli with different disparities were generated by shifting a pair of fixed patterns relative to each other by different horizontal distances. The complex cell responses were computed by averaging over adjacent quadrature pairs through a 2D Gaussian weighting function with σ_w equal to 2 pixels. This means that the RF dimension of the complex cell is 25% larger than that of the constituent simple cells. The simulation results shown in Fig. 5 are in good agreement with our analytical derivations plotted in Fig. 4; both indicate that the cell has a CD at 1°.

——— Place Fig. 5 about here ———

The calculated tuning curves in Fig. 5 are very similar to those of the example cell shown in Fig. 2 of Wagner and Frost (1993). A difference, however, is that in Fig. 5, one set of the

peaks in the grating tuning curves coincide exactly at the CD location, while for the real cell (Fig. 2 in Wagner and Frost (1993)), the peak of the curve with the lowest of the three spatial frequencies is significantly shifted rightward. We will return to this point below.

2.4 Complex cells with phase-parameter based RF model

Similarly, we can calculate the disparity tuning curves for complex cells with the phase-parameter based RFs described by Equations 1 and 2. The details of our mathematical analyses are presented in the Appendix. The response of a complex cell to a spatial noise pattern with disparity D is found to be:

$$r_{c,noise}^{phs} \approx 16\pi^2\rho^2 exp[-\frac{D^2}{4\sigma^2}]cos^2[\frac{\omega_0}{2}(D - \frac{\Delta\phi}{\omega_0})] \tag{13}$$

where

$$\Delta\phi = \phi_l - \phi_r \ . \tag{14}$$

Here ρ is again the constant Fourier amplitude of the noise stimulus. σ, ω_0 and $\Delta\phi$ are the intrinsic parameters of the simple cells used to construct the complex cell. They are the Gaussian width, the preferred spatial frequency and the left-right phase parameter difference of the simple cells. A plot of this equation is shown in Fig. 6 (part a).

——— Place Fig. 6 about here ———

The cosine term in Equation 13 is similar to that of Equation 11; it has peaks located periodically at $D = \Delta\phi/\omega_0 \pm 2\pi n/\omega_0$ where $n = 0, 1, 2, \cdots$. The ratio $\Delta\phi/\omega_0$ here is equivalent to the shift d of the position-shift model. Unlike Equation 11, however, the Gaussian term in Equation 13 is always centered at $D = 0$. Consequently, the main peak of Equation 13 is the peak of the cosine term that is closest to $D = 0$. Since the cosine term has peaks occurring periodically with a period equal to the preferred spatial period of the cell ($2\pi/\omega_0$), the main peak has to fall in the range $[-\pi/\omega_0, \pi/\omega_0]$. We conclude that for a complex cell with the phase-parameter based RF model, the main peak of its noise disparity tuning curve is always larger than the negative half preferred spatial period and smaller than the positive half preferred spatial period of the same cell. This relation is shown schematically in Fig.7. Such a constraint does not exist for complex cells with the position-shift based RF model. Note that a constraint similar to that shown in Fig. 7 has been proposed previously by Marr and Poggio (1979). However, we derived the constraint by analyzing a physiologically determined complex cell model while they reached the conclusion through the non-physiological procedure of explicitly matching the zero-crossings in the left and right images (see Qian (1994a)).

——— Place Fig. 7 about here ———

Since Equation 13 is invariant when $\Delta\phi$ is replaced by $\Delta\phi + 2\pi$, without loss of generality we can restrict $\Delta\phi$ to be within the range $[-\pi, \pi]$. Under this convention, the main peak of Equation 13 will always be at $D = \Delta\phi/\omega_0$, and the side peaks at $D = \Delta\phi/\omega_0 \pm 2\pi n/\omega_0$ where $n = 1, 2, \cdots$. We will adopt this convention for the rest of the paper. The side peaks decay away with increasing disparity D according to the Gaussian term in Equation 11.

The response of the phase-parameter based complex cell to a sinusoidal grating with spatial frequency Ω is given by (see the Appendix):

$$r_{c,sin}^{phs} = c^2 exp[-\frac{(\Omega - \omega_0)^2\sigma^2}{2}]cos^2[\frac{\Omega}{2}(D - \frac{\Delta\phi}{\Omega})]. \tag{15}$$

A plot of Equation 15 is shown in Fig. 6 (part b). According to this equation, for gratings with frequency Ω, one peak of the disparity tuning curve occurs at $D = \Delta\phi/\Omega$. Unlike complex cells with the position-shift based RFs (see Equation 12), this peak location is not completely determined by the intrinsic parameters of the cell, but depends on the grating frequency Ω. Consequently, the peaks of tuning curves from gratings of different frequencies will not coincide. Therefore, strictly speaking one cannot define a CD for complex cells with the phase-parameter based RF descriptions. However, Equation 15 has a Gaussian term which determines the spatial frequency tuning of the cell; only those gratings with frequencies (Ω's) around the preferred frequency (ω_0) of the cell can elicit good responses from the cell. If one only probes the cell with Ω's around ω_0 in order to get good responses, then one set of peaks of the grating tuning curves will be distributed closely around the disparity $\Delta\phi/\omega_0$. Since this is also the location of the main peak of the disparity tuning curve to noise patterns, for practical purposes we can define an approximate CD equal to $\Delta\phi/\omega_0$ for complex cells with the phase-parameter based RFs. Note that the above argument relies on the fact that real V1 cells are usually very well tuned to their preferred spatial frequencies. For complex cells with broader frequency tuning, the CD will become less well defined under the phase-parameter model.

To see the above argument more clearly, we have plotted the normalized disparity tuning curves to spatial noise patterns and to sinusoidal gratings of three different frequencies using the analytical expressions in Equations 13 and 15 (see Fig. 6). The set of cell parameters were chosen to closely match those used in Figs. 4 and 5 for the position-shift case. Specifically, the Gaussian width (σ) and the preferred spatial frequency ($\omega_0/2\pi$) are the same as those used in Figs. 4 and 5. The left-right phase parameter difference $\Delta\phi$ is $\pi/2$ so that the expected CD ($\Delta\phi/\omega_0$) of the complex cell is 1°, same as the CD value in Figs. 4 and 5. As can be seen from the figure, the cell indeed has an approximate CD of 1°.

The tuning curves in Fig. 6 capture the main features of the example cell in Wagner and Frost (1993). We therefore conclude that the mere existence of an approximate CD in real cells should not be taken as evidence against the phase-parameter based RF description. Note that there is a systematic deviation of the peak locations around the CD for the grating disparity tuning curves: the peak location shifts rightward with decreasing spatial frequency of the grating. (For negative CDs, the peak locations will shift leftward with decreasing spatial frequency.) A similar deviation is also present in the example cell reported by Wagner and Frost (1993). This systematic deviation is not predicted by complex cells with the position-shift based RF description. In the expanded version of their paper, Wagner

and Frost (1994) showed in their Fig. 9b that the peaks of the sinusoidal tuning curves shift with the grating frequency for the majority of the cells.

The peak deviations of the grating disparity tuning curves can be easily understood based on the above discussions of Equation 15. Note that the CD is defined at the peak location of the noise disparity tuning curve $\Delta\phi/\omega_0$ while the peaks of the grating disparity tuning curves actually occur at $\Delta\phi/\Omega$. Therefore, for the grating tuning curve with a spatial frequency Ω smaller (larger) than the preferred frequency ω_0 of the cell, its peak location around the CD will be further away from (nearer to) $D = 0$ than the CD. For the grating tuning curve with a frequency Ω equal to the preferred frequency ω_0 of the cell, it has a peak precisely at the CD. Again, we performed numerical simulations in order to check the accuracy of our analyses. The simulation results (not shown) are in good agreement with our theoretical analyses.

2.5 How to distinguish the two types of RF models?

We concluded above that the existence of an approximate CD in real cells should not be taken as evidence for rejecting the phase-parameter based RF description. Our results also suggest methods for correctly distinguishing the two RF models. One method is to examine whether the peaks of grating tuning curves align precisely at the CD as shown in Figs. 4 and 5, or the alignment is only an approximate one with a systematic deviation as shown in Fig. 6. If the systematic deviation exists in a real complex cell, this is clear evidence that the cell cannot be described by a purely position-shift based RF model since such a model always predicts a precise alignment. A potential problem with this method is that errors in the experimental measurements may render such a comparison impossible. This problem can be alleviated by recording from cells with high firing rates, and by using high contrast gratings with frequencies as different from the preferred frequency of the cell as possible.

The second method is to examine the relation between the CD and the preferred spatial period $(2\pi/\omega_0)$ of the same complex cell. As we discussed in relation to Equation 13, with the phase-parameter based RF description the main peak (and therefore the CD) of a complex cell's noise tuning curve is always in the range $[-\pi/\omega_0, \pi/\omega_0]$ (see Fig. 7). Such a constraint between the CD and the preferred spatial period does not exist for the position-shift based RF description. If a cell's CD and preferred spatial frequency violates this constraint, this is a clear indication that the cell's RF cannot be described by a purely phase-parameter type of RF model. On the other hand, if the constraint is obeyed by the real cell the situation is less conclusive; one can always argue that although the position-shift type of RF does not impose such a relationship, it could happen by chance or it could be due to some other reasons. However, if the CDs of a large population of real cells all satisfy the constraint, this would be strong evidence for the phase-parameter based RF model.

The third method for distinguishing the two RF models is by comparing the heights of the two side peaks surrounding the main peak in the noise tuning curve. The position-shift model predicts an equal decay of amplitude on either side of the main peak (see Equation 11 and Fig. 4) while the phase-parameter model predicts that the side peak closer to zero disparity should be higher than the one further away since the Gaussian decay term is centered at zero

disparity (see Equation 13 and Fig. 6). Furthermore, the phase-parameter model predicts that the height difference between the two side peaks should increase with the value of CD, decrease with the receptive size, and decrease with the preferred spatial frequency. Although the stochastic nature of the spatial noise pattern may by itself introduce some small variations in the heights of the side peaks (see the simulated noise tuning curve in Fig. 5), it should still be possible to apply the test to a large number of real cells and to examine if there is a significant trend over the population. In this connection, it is interesting to note that when this test is applied to the three reported noise tuning curves with clear side peaks (Fig. 2 of Wagner and Frost (1993) and Figs. 7 and 8a of Wagner and Frost (1994)), in all three cases the side peaks closer to zero disparity are higher than than the one further away, suggesting that the phase-parameter model is favorable.

The results from the above tests could be contradictory, with some test(s) favoring one RF model and the remaining test(s) favoring the other model. If this happens, a hybrid RF model should then be considered.

2.6 A hybrid RF model with position shift and phase parameters

It should be noted that the experiments by Freeman et al. were performed on anesthetized cats. Consequently, the absolute spatial correspondence between the left and right RF profiles of a cell cannot be accurately determined although the shape of each RF profile can be measured with high precision. It is only an assumption that the two Gaussian envelopes are aligned exactly at the corresponding retinal positions. It is therefore possible that real complex cells may use a combination of the phase-parameter and position-shift based binocular RFs to encode disparity. It can be shown that for a complex cell constructed from such a hybrid RF model, the disparity tuning functions to noise patterns and sine wave gratings can be obtained by replacing D in Equations 13 and 15 by $(D-d)$:

$$r_{c,noise}^{mix} \approx 16\pi^2\rho^2 exp[-\frac{(D-d)^2}{4\sigma^2}]cos^2[\frac{\omega_0}{2}(D-d-\frac{\Delta\phi}{\omega_0})], \tag{16}$$

$$r_{c,sin}^{mix} = c^2 exp[-\frac{(\Omega-\omega_0)^2\sigma^2}{2}]cos^2[\frac{\Omega}{2}(D-d-\frac{\Delta\phi}{\Omega})]. \tag{17}$$

Thus, if one probes the cell with grating frequencies (Ω's) around the cell's preferred frequency (ω_0), the cell will appear to have an approximate CD equal to the sum of the contributions from the positional shift and the phase parameters: $CD \approx d + \Delta\phi/\omega_0$. There will still be a systematic deviation of the peak locations around the CD for the grating disparity tuning curves but the relative deviation with respect to the magnitude of CD will be smaller than that in a purely phase-parameter based approach because now the phase parameters only contribute part of the total CD. For a fixed d, the value of the CD will now fall in the range of $[d-\pi/\omega_0,\ d+\pi/\omega_0]$; the constraint shown in Fig. 7 should be displaced along the vertical axis by d.

For real complex cells, it is also easy to estimate the relative contributions of the position shifts and phase parameters to their disparity tuning. Assume a cell's disparity tuning is generated by a position shift d and a phase parameter difference $\Delta\phi$ between its left and right RFs. By measuring the peak location (D_1) of its disparity tuning curve to spatial noise patterns, we have the relation:

$$D_1 = d + \frac{\Delta\phi}{\omega_0} \tag{18}$$

according to Equation 16. Next, we measure the peak location (D_2) of one grating tuning curve (with grating frequency Ω) near the CD and have another equation:

$$D_2 = d + \frac{\Delta\phi}{\Omega} \tag{19}$$

according to Equation 17. The preferred spatial frequency ω_0 of the cell can be measured separately from the cell's spatial frequency tuning curve, or it can be estimated from the spacing between the peaks in the noise disparity tuning curve (which is equal to $2\pi/\omega_0$ according to Equation 16). We can therefore solve for d and $\Delta\phi$ from the above two equations.

It is interesting to note that the example cell in Wagner and Frost (1993) can be best modeled by a mixed RF description. That cell showed a deviation in the peak locations around the CD in its grating tuning curves. It therefore cannot be explained by a pure position-shift based RF model. In addition, its CD was larger than half of its preferred spatial period (the preferred spatial period of the cell was not stated by the authors, but it should be approximately equal to the period of its noise tuning curve according to Equation 16), and therefore cannot be explained by a purely phase-parameter based RF model. Only a hybrid model can account for both aspects. We have performed computer simulations to model the tuning curves of this cell with the mixed RF descriptions. The left-right phase difference $\Delta\phi$ is chosen to be $\pi/2$ and the position shift parameter d is 1.5°. These parameters were determined according to the method described in the previous paragraph (D_2 was measured from the grating tuning curve with the lowest spatial frequency). The Gaussian width σ is set to be 1° and the preferred spatial frequency ($\omega_0/2\pi$) is 0.5 cycle/degree. The results are shown in Fig. 8. The cell has an approximate CD of 2°, as expected based on our analyses. The tuning curves compare well with those of the real cell in Fig. 2 of Wagner and Frost (1993). Although this demonstrates the requirement of a hybrid model for describing the RF profiles of this particular cell, a general conclusion can only be drawn after examining a large number of real cells.

In the expanded version of their paper, Wagner and Frost (1994) reported recordings from a few more cells. Unfortunately, none of the recordings contained a complete set of tuning curves to allow a similar analysis as we did above. For example, their Fig. 6 does not contain the cell's noise tuning curve, which is needed in order to determine the CD location and the preferred spatial frequency of the cell. Their Fig. 10 showed a cell's noise tuning curve but only one grating tuning curve. If the spatial frequency of the grating was the cell's preferred frequency then the phase-parameter model would also predict that the main peak of the noise tuning curve should line up with one of the peaks in the grating tuning curve.

——— Place Fig. 8 about here ———

2.7 An examination of Wagner and Frost's data analysis

In addition to our suggestions of possible experiments for distinguishing the two RF models, our theoretical results can also be used to examine the data analysis method presented in Fig. 3 of Wagner and Frost (1993). The authors first fitted each experimentally measured grating tuning curve with a cosine function of the form

$$cos[\Omega_i D + \Phi_i] \tag{20}$$

where Ω_i and Φ_i are the frequency and phase of the ith grating tuning curve. Clearly, Ω_i should be equal to the spatial frequency of the gratings used to obtain the ith grating tuning curve. They then calculated a mean disparity value (called MD in their paper) by using the main peak location of the noise tuning curve and the peaks of the grating tuning curves near the main peak. After that, they estimated the phase (called MP in the paper) predicted by the phase-parameter and the position-shift models according to

$$MP_{phase} = MD * \omega_0 \tag{21}$$

$$MP_{position} = MD * \Omega_i \tag{22}$$

where ω_0 is the preferred spatial frequency of the cell. Finally, for the cells they recorded, they calculated the squared deviations between the measured phases Φ_i and the predicted phases (MP) for each RF model. Since the deviation for the phase-parameter model is larger than that for the position-shift model, they concluded that the position-shift model is preferable (see Fig. 3(b) of Wagner and Frost (1993)).

We now examine their analysis in light of our theoretical results. First, under the assumption of the position-shift RF model, the mean disparity MD should simply be the relative shift d between the left and right RFs. The predicted phase $MP_{position}$ is therefore equal to $\Omega_i d$. This is the correct phase of the grating tuning curve according to our Equation 12. On the other hand, if we assume the phase-parameter model is correct, MD can be expressed as (see Equations 13 and 15)

$$MD = \frac{\frac{\Delta\phi}{\omega_0} + \sum_{i=1}^{N} \frac{\Delta\phi}{\Omega_i}}{N+1} \tag{23}$$

where N is the number of grating tuning curves used in the calculation. Therefore, MP_{phase} does not yield the correct predicted phase of the grating tuning curve, which should be $\Delta\phi$ according to our Equation 15, unless

$$\frac{\frac{1}{\omega_0} + \sum_{i=1}^{N} \frac{1}{\Omega_i}}{N+1} \approx \frac{1}{\omega_0} \ . \tag{24}$$

Unfortunately, this relation is not generally satisfied. Assuming that in the actual experiments, Ω_i's were chosen symmetrically around the preferred frequency ω_0, one can then show

that MP_{phase} gives an overestimation of the phase in the grating tuning curves because

$$\frac{\frac{1}{\omega_0}+\sum_{i=1}^{N}\frac{1}{\Omega_i}}{N+1} > \left(\frac{\omega_0+\sum_{i=1}^{N}\Omega_i}{N+1}\right)^{-1} = \frac{1}{\omega_0} \tag{25}$$

(The inequility can be proved for any positive ω_0 and Ω_i that are not all identical to each other.) Since the squared deviation (Wagner and Frost, 1993) of the phase-parameter model is already quite small (although larger than that of the position-shift model), even a small bias in the estimation of the model prediction could have significant consequences. Obviously, the correct calculation of the predicted phase under the phase-parameter model should only use the main peak location of the noise tuning curve.

There is a potentially more fundamental problem with the data analysis in Fig. 3 of Wagner and Frost (1993): the authors did not first classify cells into simple and complex and then exclude simple cells from their CD analysis. As we have shown, although one can measure disparity tuning curves from simple cells, their CDs are undefined no matter which RF model one chooses. In addition, in the expanded version of Wagner and Frost (1993) the authors mentioned that during their experiments, "single units were difficult to isolate", and that the majority of the recordings were multi-unit (Wagner and Frost, 1994). Consequently, many of their measured tuning curves were the average from several different cells. It is inappropriate to apply CD analysis to multi-unit recordings unless the cells in a given recording were all complex and all had identical disparity tuning. We conclude that the existing physiological data by Wagner and Frost does not allow a clear distinction of the two RF models.

3 Discussion

In this paper, we have thoroughly analyzed the disparity tuning behavior of binocular simple and complex cells with both the position-shift based and the phase-parameter based RF descriptions. Besides the general interest of relating disparity tuning behavior of a cell to its RF structures, our work also addresses the specific question of which cell type and RF structure are most consistent with the CD data by Wagner and Frost (1993). We have derived analytical expressions for the disparity tuning curves for both simple and complex cells with either type of RF model. We have also confirmed our analyses through computer simulations. Our results indicate that simple cells with either type of RF model cannot have a CD because these cells do not even have well-defined disparity tuning curves due to their dependence on stimulus Fourier phases. Model complex cells, on the other hand, do not suffer from this phase problem and have reliable disparity tuning curves. Furthermore, model complex cells with the position-shift based RF description have a precise CD, and those with the phase-parameter based RF description have an approximate CD. A testable prediction is that real cells found to have CDs should all be complex cells. We concluded based on these results that the mere existence of (approximate) CDs in real cells cannot be used to distinguish the phase-parameter based RF description from the traditional position-shift based RF description.

It should be clarified that when we say simple cells do not have well-defined disparity tuning curves we do not mean that they do not have measurable disparity tuning; real simple

cells do have disparity tuning (Bishop et al., 1971; Poggio and Fischer, 1977). Rather, we mean that their disparity tuning curves change dramatically when the same type of stimuli with different Fourier phases are used in the measurements (see Fig. 2). There is experimental evidence suggesting that this is indeed the case. For example, Ohzawa et al. (1990) showed that disparity tuning curves of a simple cell measured with bright bars and dark bars are different (see also the Discussion in Qian (1994a)).

The simple cell model used in our analyses and simulations is identical to those proposed by Freeman et al. (Freeman and Ohzawa, 1990; Ohzawa et al., 1990). The complex cell model we used, on the other hand, differs slightly from theirs. One difference is only superficial: they separated the positive and negative responses of simple cells and therefore had four simple-type subunits in a quadrature pair while we did not do the separation explicitly and had two simple cells in a quadrature pair. Mathematically, the two approaches are exactly equivalent. The real (and only) difference between our complex cell model and theirs is that we added a final spatial pooling step (see Equation 10). The response of our model complex cell is therefore a weighted average of several quadrature pairs with nearby and overlapping RFs. Our analytical and simulation results (not shown) indicate that for the disparity tuning curves of bar stimuli measured and modeled by Freeman et al., adding the spatial pooling step or not does not make any difference. For spatial noise patterns, however, the disparity tuning curves computed with the pooling step added are much more reliable and independent of stimulus Fourier phases than without the pooling step (see the Appendix). Therefore, by experimentally testing the reliability of disparity tuning to noise patterns one could potentially determine whether the spatial pooling operation is indeed employed by real complex cells. Also note that spatial pooling is just one of the pooling methods widely used in the computer vision literature. One could also pool responses across different spatial frequency scales (Marr and Poggio, 1979; Grzywacz and Yuille, 1990; Fleet, Heeger and Wagner, 1995). However, we think spatial pooling is a natural choice for modeling complex cells because it accounts for the larger RF sizes of real complex cells, and at the same time it preserves complex cells' frequency tuning properties. In contrast, pooling across different spatial frequency scales would render complex cells much less sensitive (i.e., more broadly tuned) to spatial frequency than simple cells, contradictory to the actual experimental data (Shapley and Lennie, 1985). Frequency pooling is therefore most likely to occur at a stage beyond complex cells, perhaps at the level of MT (Grzywacz and Yuille, 1990).

We have previously developed a physiologically realistic algorithm for disparity computation using the phase-parameter based RF description (Qian, 1994a). The algorithm relies on the same simple and complex cell response models as described in this paper, and uses a population of complex cells to encode stimulus disparity. In fact, Equation 13 in this paper is a more accurate derivation of the complex cell response than Equation 2.8 in Qian (1994a). The only difference between the complex cell model presented here and the one used in Qian (1994a) is that we have added a spatial pooling step in this paper (see Equation 10). As we mentioned above, this step accounts for the larger RF sizes of complex cells compared with simple cells, and makes the disparity tuning curves of complex cells more reliable. The quality of the computed disparity maps from random dot stereograms with the pooling step added is significantly better than those without the pooling step, especially at disparity boundaries (Qian and Zhu, 1995).

Our algorithm for disparity computation also works with the position-shift based RF

description since Equation 11 indicates that a population of complex cells with the position-shift based RF models can also form a distributed representation of stimulus disparity. We have performed computer simulations using the algorithm with both types of RF models. The computed disparity maps from random dot stereograms (Qian, 1994a) using the two different RF models are very similar to each other, both agree well with the actual disparity map (results not shown). However, under certain conditions, the computed disparity maps using different RF models may be somewhat different. This is the case for sinusoidal grating stimuli. Our analyses indicate that for sinusoidal gratings of any frequencies, the position-shift based algorithm should always give the actual disparity value of the stimuli (within one spatial period of the gratings). For the algorithm based on the phase parameters, on the other hand, the disparity of those gratings with high spatial frequencies will be underestimated while those with low frequencies will be overestimated. This result provides an opportunity for distinguishing the two types of RF models via visual psychophysical experiments.

One major limitation with the simple and complex cell models we used is that their responses are monotonic functions of stimulus contrast and therefore they do not account for the contrast saturation behavior of real cells. This problem, however, can be readily fixed with a normalization procedure (Albrecht and Geisler, 1991; Heeger, 1992). Indeed, normalization methods have already been used by Fleet et al. (1995) to account for experimental data on binocular contrast effects. The introduction of normalization will not affect conclusions of this paper, however, because the normalization factor is a function of contrast but not a function of disparity (because it is obtained by summing over cells with all preferred disparities) and therefore will not change the peak locations of disparity tuning curves. Likewise, the normalization procedure will not affect our recent algorithm (Qian, 1994a) for disparity computation either since the algorithm only relies on the location of peak disparity responses.

We have also suggested new methods for distinguishing the phase-parameter based and the position-shift based RF models. One method relies on the fact that the CD of the complex cells with the phase-parameter based RF models can only be defined approximately. The peaks of the sinusoidal tuning curves spread around the main peak of the noise tuning curve in a systematic way. This type of systematic deviation is not predicted by the position-shift based RF model. The second method observes that for the phase-parameter based RF model the CD of a complex cell has to occur in a range restricted by the preferred spatial period of the cell while this restriction does not apply to the position-shift based RF model. The third method compares the side peak heights in the noise tuning curve. We suggest that by applying these methods to a large number of real cells, a better understanding of the binocular RF structure could be obtained. If conflicting results are obtained with these methods, one should then consider the hybrid RF model containing both a position shift and a phase parameter difference between the left and right RFs. We showed how to determine the relative contributions of the position shift and the phase parameter difference for real complex cells.

In conclusion, our work provides a thorough characterization of the disparity tuning of simple and complex cells under the two different types of RF descriptions (and their hybrid) suggested by previous physiological experiments. These results not only provide an explanation of many aspects of the recent physiological data of (Wagner and Frost, 1993) but also generate specific predictions which may help guide future experimental determination

of the neural mechanisms of disparity selectivity.

Appendix

We outline our derivation of the simple and complex cell response functions for the phase-parameter and the position-shift based RF models in this Appendix. For an arbitrary stimulus with a disparity D, its left and right retinal images can be written as:

$$\begin{aligned} I_l(x) &= I(x) \ , \\ I_r(x) &= I(x+D) \ . \end{aligned} \tag{26}$$

According to the Fourier theorem, a function $I(x)$ and its Fourier transform $\tilde{I}(\omega) \equiv \mathcal{F}(I(x))$ are related by:

$$I(x) = \int d\omega \tilde{I}(\omega) e^{i\omega x} \ . \tag{27}$$

In general, $\tilde{I}(\omega)$ takes complex value and can be expressed by an amplitude $\rho(\omega)$ and a phase $\theta(\omega)$,

$$\tilde{I}(\omega) = \rho(\omega) e^{i\theta(\omega)} \ . \tag{28}$$

In addition, the Fourier transform of $I(x+D)$ is:

$$\mathcal{F}(I(x+D)) = \tilde{I}(\omega) e^{i\omega D} \ . \tag{29}$$

based on the definition of Fourier transform. Substituting the above relations into the simple cell response model of Equation 5, we have:

$$r_s = \int d\omega \int dx \rho(\omega) e^{i\theta(\omega)+i\omega x} [f_l(x) + e^{i\omega D} f_r(x)] \ . \tag{30}$$

It should be pointed out that we do not assume that the cortical cells perform Fourier transformations. The technique is used in our calculations merely as a mathematical tool to analyze cells' responses.

When the RF profiles, $f_l(x)$ and $f_r(x)$, are specified, the spatial dependence of the integrand in Equation 30 is completely known. This allows us to carry out the integration over the variable x. For the position-shift based RF model, the RF profiles are given by Equations 3 and 4. Substituting them into Equation 30, we found that with the position-shift based RF model the simple cell response to an arbitrary stimulus of disparity D is given by:

$$\begin{aligned} r_s^{pos} &= 2\sqrt{2\pi\sigma^2} \int_{-\infty}^{+\infty} d\omega \rho(\omega) e^{-(\omega-\omega_0)^2\sigma^2/2} cos[\frac{1}{2}\omega(D-d)] \times \\ & \qquad cos[\phi - \theta(\omega) - \frac{1}{2}\omega(D-d)] \end{aligned} \tag{31}$$

We have used the following identity in deriving the above equation:

$$\int_{-\infty}^{\infty} dx e^{-\frac{x^2}{2\sigma^2}} e^{-iax} = \sqrt{2\pi\sigma^2} e^{-a^2\sigma^2/2} \ . \tag{32}$$

Similarly, the simple cell response under the phase-parameter based RF model can be derived as

$$\begin{aligned} r_s^{phs} &= 2\sqrt{2\pi\sigma^2}\int_{-\infty}^{+\infty} d\omega\rho(\omega)e^{-(\omega-\omega_0)^2\sigma^2/2}cos[\frac{1}{2}(\omega D-\Delta\phi)] \\ &\quad cos[\frac{1}{2}(\phi_l+\phi_r-\omega D)-\theta(\omega)]. \end{aligned} \tag{33}$$

Note that both Equations 31 and 33 are dependent on the Fourier phase $\theta(\omega)$ of the external stimulus. This means that with a fixed disparity D, any change to the external stimulus that results in variation of its Fourier phase will effectively alter the response of simple cells. We therefore conclude that simple cells do not have reliable disparity tuning. An approximate version of Equation 33 was derived in Qian (1994a).

Using the definition of a quadrature pair in Equations 6 to 9 and the above simple cell response expressions we found that the output of a quadrature pair of simple cells with the position-shift based RF model is given by

$$\begin{aligned} r_q^{pos} &= [r_s^{pos}(\phi)]^2+[r_s^{pos}(\phi+\pi/2)]^2 \\ &= 8\pi\sigma^2\int\int d\omega d\omega'\rho(\omega)\rho(\omega')e^{-(\omega'-\omega_0)^2\sigma^2/2}e^{-(\omega-\omega_0)^2\sigma^2/2}\times \\ &\quad cos[\frac{\theta(\omega')-\theta(\omega)}{2}+\frac{(\omega-\omega')(D-d)}{2}]cos[\frac{\omega}{2}(D-d)]cos[\frac{\omega'}{2}(D-d)], \end{aligned} \tag{34}$$

where we have converted the squares of integration into double integrations. Similarly, the output of a quadrature pair of simple cells with the phase-parameter based RF model is given by

$$\begin{aligned} r_q^{phs} &= [r_s^{phs}(\phi_l,\phi_r)]^2+[r_s^{phs}(\phi_l+\pi/2,\phi_r+\pi/2)]^2 \\ &= 8\pi\sigma^2\int\int d\omega d\omega'\rho(\omega)\rho(\omega')e^{-(\omega-\omega_0)^2\sigma^2/2}e^{-(\omega'-\omega_0)^2\sigma^2/2}\times \\ &\quad cos[\frac{\theta(\omega')-\theta(\omega)}{2}+\frac{(\omega-\omega')D}{2}]cos[\frac{1}{2}(\Delta\phi-\omega D)]cos[\frac{1}{2}(\Delta\phi-\omega' D)]. \end{aligned} \tag{35}$$

According to these expressions, the responses of a quadrature pair differ from that of the simple cells in that they depend on the difference of the Fourier phases of the input stimulus measured at two different frequencies ($\theta(\omega')-\theta(\omega)$). Both integrands contain two Gaussian factors that are significantly large only when both ω and ω' are approximately equal to ω_0. This effectively makes $\omega'-\omega$ very small. It also makes $\theta(\omega')-\theta(\omega)$ close to zero for the stimuli whose Fourier phases are smooth functions of frequency (such as lines, bars or gratings) . We can therefore neglect the θ dependence in the above two equations for these stimuli by assuming

$$cos[\frac{\theta(\omega')-\theta(\omega)}{2}+\frac{(\omega-\omega')(D-d)}{2}]\approx const, \tag{36}$$

$$cos[\frac{\theta(\omega')-\theta(\omega)}{2}+\frac{(\omega-\omega')D}{2}]\approx const\ . \tag{37}$$

However, $\theta(\omega)$ is not a smooth function of ω for stimuli like the spatial noise patterns, and this is when the final pooling step for computing complex cell responses (see Equation 10) becomes important. In this pooling step the responses of many quadrature pairs with nearby RFs (and with otherwise identical parameters) are averaged. The response expressions (Equation 34 or 35) for the different quadrature pairs are identical except the $\theta(\omega)$ functions which are different for different pairs because they are centered on somewhat different parts of the noise stimuli. Therefore, the pooling step simply averages over the θ dependent cosine terms in Equation 34 or 35, and makes them approximately constant (as long as the stimulus patches covered by the pooled quadrature pairs contain many independent θ's). The approximations in Equations 36 and 37 are thus also valid for the noise stimuli after the pooling.

Using Equations 36 and 37, we can now reduce Equations 34 and 35 to:

$$\begin{aligned} r_c^{pos} &\approx 8\pi\sigma^2 \int\int d\omega d\omega' \rho(\omega)\rho(\omega') e^{-(\omega-\omega_0)^2\sigma^2/2} e^{-(\omega'-\omega_0)^2\sigma^2/2} \times \\ &\quad cos[\frac{\omega}{2}(D-d)] cos[\frac{\omega'}{2}(D-d)], \end{aligned} \tag{38}$$

and

$$\begin{aligned} r_c^{phs} &\approx 8\pi\sigma^2 \int\int d\omega d\omega' \rho(\omega)\rho(\omega') e^{-(\omega-\omega_0)^2\sigma^2/2} e^{-(\omega'-\omega_0)^2\sigma^2/2} \times \\ &\quad cos[\frac{1}{2}(\Delta\phi - \omega D)] cos[\frac{1}{2}(\Delta\phi - \omega' D)] \end{aligned} \tag{39}$$

Equations 38 and 39 are the complex cell responses to a stimulus with disparity D, for the position-shift and the phase-parameter based RF models respectively. Unlike simple cell response functions in Equations. 31 and 33, both of these complex cell response functions are independent of the stimulus Fourier phase. Complex cells should therefore have reliable disparity tuning curves. This conclusion is true for both the position-shift and the phase-parameter based RF models.

To investigate CDs of complex cells, we need to derive their disparity tuning curves for spatial noise patterns and sine wave gratings. A noise pattern has a broad Fourier spectrum, and its Fourier amplitude $\rho(\omega)$ is a constant ρ independent of ω. On the other hand, the Fourier transform of a sine wave grating contains only two frequency components. For a grating with frequency Ω, its transform is given by

$$\mathcal{F}(sin(\Omega x)) = \frac{i}{2}(\delta(\Omega+\omega) - \delta(\Omega-\omega)) \tag{40}$$

where $\delta()$ is the Dirac δ-function and is nonzero only when its argument is zero. Using these properties in conjunction with Equations 38 and 39, it is easy the derive Equations 11 and 12 in the text for the position-shift based RF model, and Equations 13 and 15 for the phase-parameter based RF model. It should be pointed out that our analyses include approximations of Equations 36 and 37. Their validity has been confirmed by our computer simulations. Actually, these two approximations are not necessary for deriving tuning curves to sinusoidal gratings. The special property of these stimuli shown in Equation 40 makes it possible to derive their tuning curves (Equations 12 and 15) exactly. This explains why the grating disparity tuning curves predicted by our analyses are almost indistinguishable from our simulation results.

Acknowledgments

We would like to thank Drs. Terry Sejnowski and Alex Pouget for helpful discussions. The work is supported by a research grant from the McDonnell-Pew Program in Cognitive Neuroscience and NIH grant #MH54125, both to N. Q.

References

Adelson, E. H. and Bergen, J. R. (1985). Spatiotemporal energy models for the perception of motion, *J. Opt. Soc. Am. A* **2**(2): 284–299.

Albrecht, D. G. and Geisler, W. S. (1991). Motion sensitivity and the contrast-response function of simple cells in the visual cortex, *Visual Neuroscience* **7**: 531–546.

Bishop, P. O. and Pettigrew, J. D. (1986). Neural mechanisms of binocular vision, *Vision Res.* **26**: 1587–1600.

Bishop, P. O., Henry, G. H. and Smith, C. J. (1971). Binocular interaction fields of single units in the cat striate cortex, *J. Phsiol.* **216**: 39–68.

DeAngelis, G. C., Ohzawa, I. and Freeman, R. D. (1991). Depth is encoded in the visual cortex by a specialized receptive field structure, *Nature* **352**: 156–159.

Ferster, D. (1981). A comparison of binocular depth mechanisms in areas 17 and 18 of the cat visual cortex, *J. Phsiol.* **311**: 623–655.

Fleet, D., Heeger, D. and Wagner, H. (1995). Computational model of binocular disparity, *Invest. Opthalmol. and Vis. Sci. Suppl. (ARVO)* **36**(4): 365.

Freeman, R. D. and Ohzawa, I. (1990). On the neurophysiological organization of binocular vision, *Vision Res.* **30**: 1661–1676.

Grzywacz, N. M. and Yuille, A. L. (1990). A model for the estimate of local image velocity by cells in the visual cortex, *Proc. R. Soc. Lond. A* **239**: 129–161.

Heeger, D. J. (1992). Normalization of cell responses in cat striate cortex, *Visual Neurosci.* **9**: 181–197.

Hubel, D. H. and Wiesel, T. (1962). Receptive fields, binocular interaction, and functional architecture in the cat's visual cortex, *J. Phsiol.* **160**: 106–154.

Jones, J. P. and Palmer, L. A. (1987). The two-dimensional spatial structure of simple receptive fields in the cat striate cortex, *J. Neurophysiol.* **58**: 1187–1211.

Marr, D. and Poggio, T. (1979). A computational theory of human stereo vision, *Proc. R. Soc. Lond. B* **204**: 301–328.

Maske, R., Yamane, S. and Bishop, P. O. (1984). Binocular simple cells for local stereopsis: comparison of receptive field organizations for the two eyes, *Vision Res.* **24**: 1921–1929.

Ohzawa, I., DeAngelis, G. C. and Freeman, R. D. (1990). Stereoscopic depth discrimination in the visual cortex: Neurons ideally suited as disparity detectors, *Science* **249**: 1037–1041.

Pettigrew, J. D. (1993). Two ears and two eyes, *Nature* **364**: 756–757.

Poggio, G. F. and Fischer, B. (1977). Binocular interaction and depth sensitivity in striate and prestriate cortex of behaving rhesus monkey, *J. Neurophysiol.* **40**: 1392–1405.

Poggio, G. F. and Poggio, T. (1984). The analysis of stereopsis, *Ann. Rev. Neurosci.* **7**: 379–412.

Qian, N. (1994a). Computing stereo disparity and motion with known binocular cell properties, *Neural Comp.* **6**: 390–404.

Qian, N. (1994b). Stereo model based on phase parameters can explain characteristic disparity, *Soc. Neurosc. Abs.* **20**: 624.

Qian, N. and Andersen, R. A. (1996). A physiological model for motion-stereo integration and a unified explanation of the Pulfrich-like phenomena. (submitted).

Qian, N. and Zhu, Y. (1995). Physiological computation of binocular disparity, *Soc. Neurosc. Abs.* **21**: 1507.

Schiller, P. H., Finlay, B. L. and Volman, S. F. (1976). Quantitative studies of single-cell properties in monkey striate cortex: I. spatiotemporal organization of receptive fields, *J. Neurophysiol.* **39**: 1288–1319.

Shapley, R. and Lennie, P. (1985). Spatial frequency analysis in the visual system, *Ann. Rev. Neurosci.* **8**: 547–583.

Wagner, H. and Frost, B. (1993). Disparity-sensitive cells in the owl have a characteristic disparity, *Nature* **364**: 796–798.

Wagner, H. and Frost, B. (1994). Binocular responses of neurons in the barn owl's visual Wulst, *J. Comp. Physiol. A* **174**: 661–670.

Watson, A. B. and Ahumada, A. J. (1985). Model of human visual-motion sensing, *J. Opt. Soc. Am. A* **2**: 322–342.

Figure 1: Profiles of the two types of binocular RF models considered in this paper. Only the horizontal dimension is considered. The dot over the vertical axis marks the peak position of the Gaussian envelopes. (a) The phase-parameter based RF model proposed by Freeman et al.(Freeman and Ohzawa, 1990; Ohzawa et al., 1990; DeAngelis et al., 1991). The left and right RF profiles (solid lines) of a binocular simple cell are assumed to be described by two Gabor functions, one for each eye, with the same Gaussian envelopes (dotted lines) but two different phase parameters in their sinusoidal modulations. The mathematical descriptions of these RFs are given by Equations 1 and 2. The difference between the left and right phase parameters ($\Delta\phi = \phi_l - \phi_r$) generates a relative shift between the left and right sinusoidal modulations within their registered Gaussian envelopes. It also creates a shape difference between the two RF profiles. (b) The traditional position-shift based RF model favored by (Wagner and Frost, 1993). The left and right RFs have identical shapes but have an overall horizontal shift d between them (i.e., the same amount of shift applies to both Gaussian envelope and sinusoidal modulation). The mathematical descriptions of these RFs are given by Equations 3 and 4. Simple and complex cells can be built with either type of RF models (see Analyses and Simulations).

Figure 2: Normalized disparity tuning curves of a simple cell with the position-shift based RF model to two sets of independently generated random dot patterns. The peak locations of the two tuning curves from the same simple cell are very different. The main peaks of both curves do not correspond to the cell's shift parameter d (marked by the verticle line). Similar results were obtained from simple cells with the phase-parameter based RF models (Qian, 1994a). Therefore, simple cells with either type of RF models do not have well-defined disparity tuning curves and cannot have a CD. The parameters used in the simulations are $\sigma = 2°$, $\omega_0/2\pi = 0.25$ cycles/degree, and the relative shift between the left and the right RFs $d = 1°$. One degree was represented by 4 pixels in the simulations. The two sets of random dot patterns both had a dot density of 50% and dot size of 1 pixel. Each set was created by horizontally shifting two identical patterns with respect to each other by different distances.

Figure 3: Normalized disparity tuning curves of a complex cell with the position-shift based RF model to two sets of independently generated random dot patterns. Unlike the simple cell shown in Fig. 2, the two tuning curves of the complex cell have very similar shapes and nearly identical peak locations. Similar results (not shown) were obtained with the phase-parameter based RF models. Therefore, complex cells with either type of RF models have well-defined disparity tuning curves. The complex cell was constructed from simple cells with the same parameters as the simple cell in Fig. 2. The spatial weighting function w (see Equation 10) was chosen to be a 2D Gaussian with a σ_w equal to 2 pixels. The random dot patterns were generated in the same way as those used in Fig. 2.

Figure 4: Normalized disparity tuning curves of a complex cell with the position-shift based RF model plotted according the analytical results in Equations 11 and 12. (a) Tuning curve to spatial noise patterns; (b) Tuning curves to sinusoidal gratings with spatial frequencies ($\Omega/2\pi$) equal to 0.154 (solid line), 0.25 (dotted line) and 0.4 (dashed line) cycles/degree respectively. The cell parameters are $\sigma = 2°$, $\omega_0/2\pi = 0.25$ cycles/degree, and the relative shift between the left and the right receptive fields $d = 1°$. These curves show a CD (marked by the vertical line) at $D = 1°$.

Figure 5: Normalized disparity tuning curves of a complex cell with the position-shift based RF model obtained through numerical simulations. (a) Tuning curve to spatial noise patterns. They were random dot patterns with a dot density of 50% and a dot size of 1 pixel. Different image disparities were generated by shifting two identical patterns with respect to each other by different distances. (b) Tuning curves to sinusoidal gratings with spatial frequencies ($\Omega/2\pi$) equal to 0.154 (solid line), 0.25 (dotted line) and 0.4 (dashed line) cycles/degree respectively. The cell parameters are identical to those used in Fig. 4. The simulated results are in good agreement with the analytical results in Fig. 4, both indicate a CD of 1°.

Figure 6: Normalized disparity tuning curves of a complex cell with the phase-parameter based RF model plotted according the analytical results in Equations 13 and 15. (a) Tuning curve to spatial noise patterns; (b) Tuning curves to sinusoidal gratings with spatial frequencies ($\Omega/2\pi$) equal to 0.154 (solid line), 0.25 (dotted line) and 0.4 (dashed line) cycles/degree respectively. The set of cell parameters were chosen to closely match those used in Figs. 4 and 5 for the position-shift case, with $\sigma = 2°$, $\omega_0/2\pi = 0.25$ cycles/degree, and $\Delta\phi = \pi/2$. These curves show an approximate CD (marked by the vertical line) at $D = 1°$. Note that the peak locations of the grating tuning curves show a systematic deviation around the CD similar to the real cell in Fig. 2 of Wagner and Frost (1993).

Figure 7: Constraint on the main peak locations (CDs) of complex cells' noise disparity tuning curves under the phase-parameter based RF model. According to Equation 13, the main peak of the noise disparity tuning curve of a cell should be larger than the negative half of its preferred spatial period and smaller than the positve half of its preferred spatial period. This constraint is represented by the two dashed lines in the figure. Each filled dot in the figure represents a hypothetical data point from a complex cell that satisfies this constraint. This constraint does not apply to complex cells with the position-shift based RF model.

Figure 8: Simulation of the disparity tuning curves of the real cell in Fig. 2 of Wagner and Frost (1993). A complex cell with a mixed RF model was used and the computed tuning curves were presented in a format similar to that for the real cell. (a) Normalized tuning curve to spatial noise patterns. The patterns were generated in the same way as those in Fig. 5. (b) Normalized disparity tuning curves to sinusoidal gratings with spatial frequencies equal to 0.25 (solid line), 0.4 (dotted line) and 0.667 (dashed line) cycles/degree respectively. These frequencies correspond to the effective grating periods (4, 2.5 and 1.5 degrees) used for the real cell. The tuning curves were deliberately truncated for better comparison with the real data. The peak locations of these curves agree well with those of the real cell.

(a) Phase-parameter based RF model

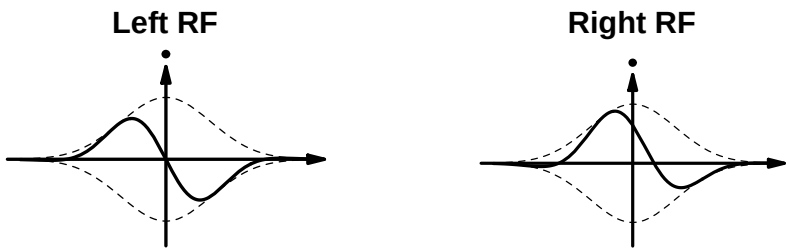

(b) Position-shift based RF model

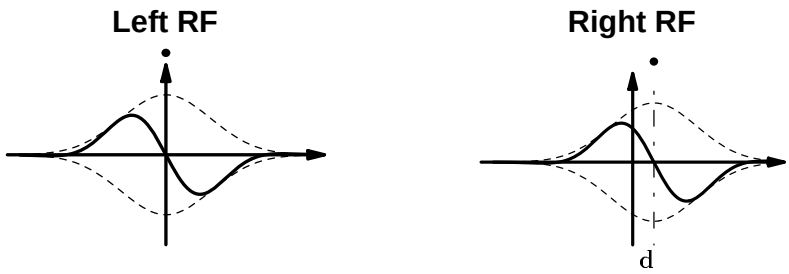

Fig.1 Zhu & Qian

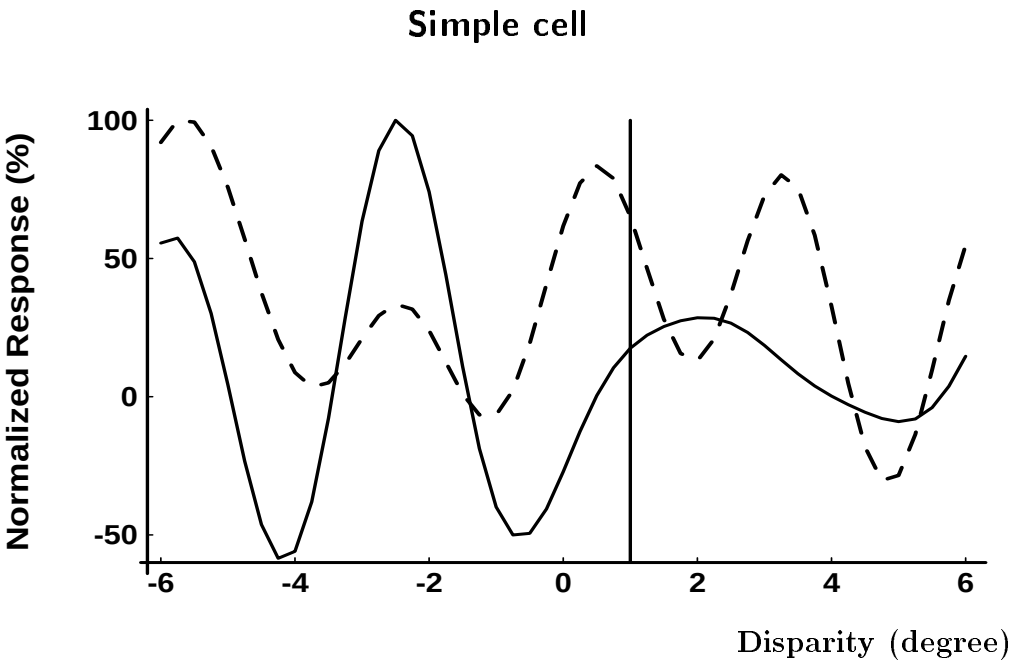

Fig.2 Zhu & Qian

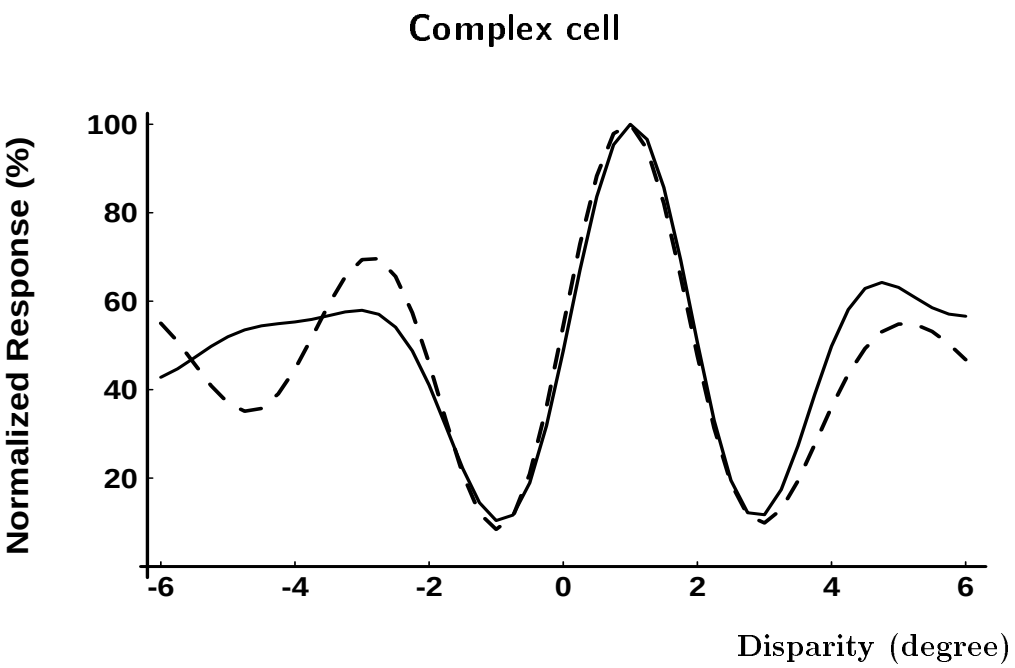

Fig.3 Zhu & Qian

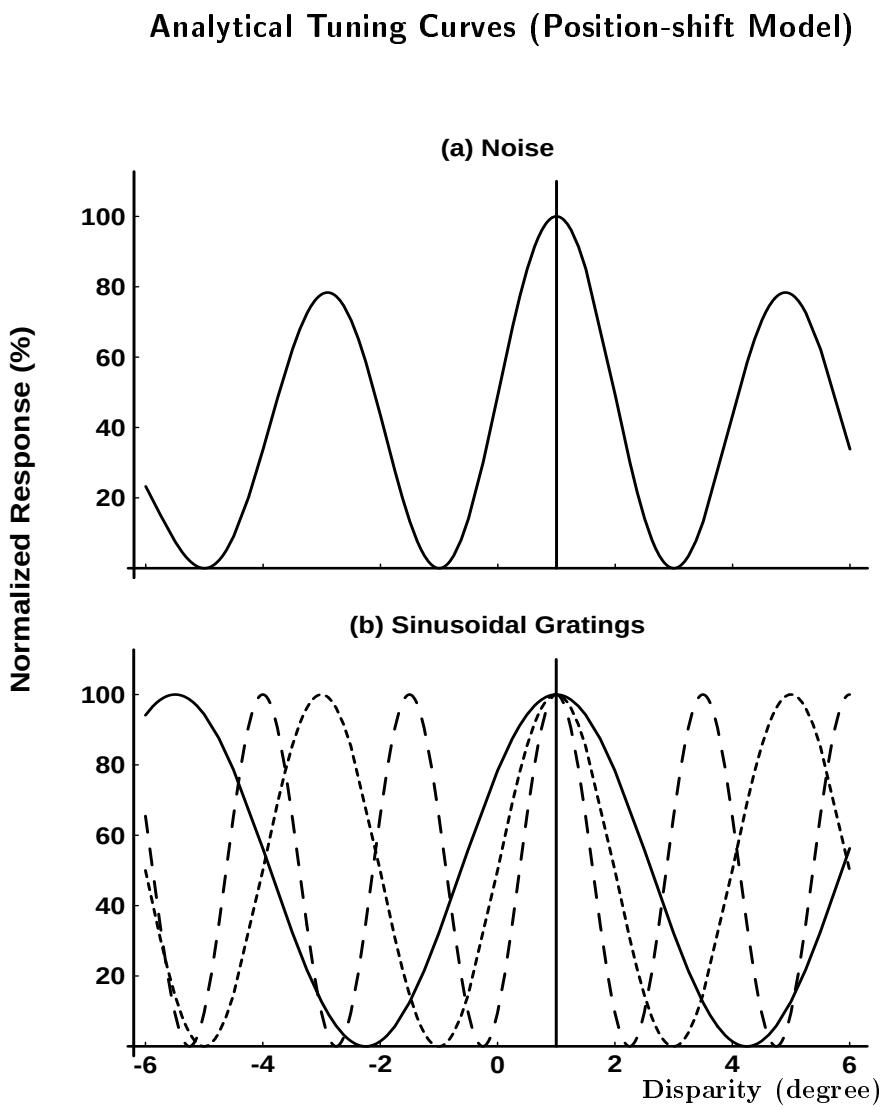

Fig.4 Zhu & Qian

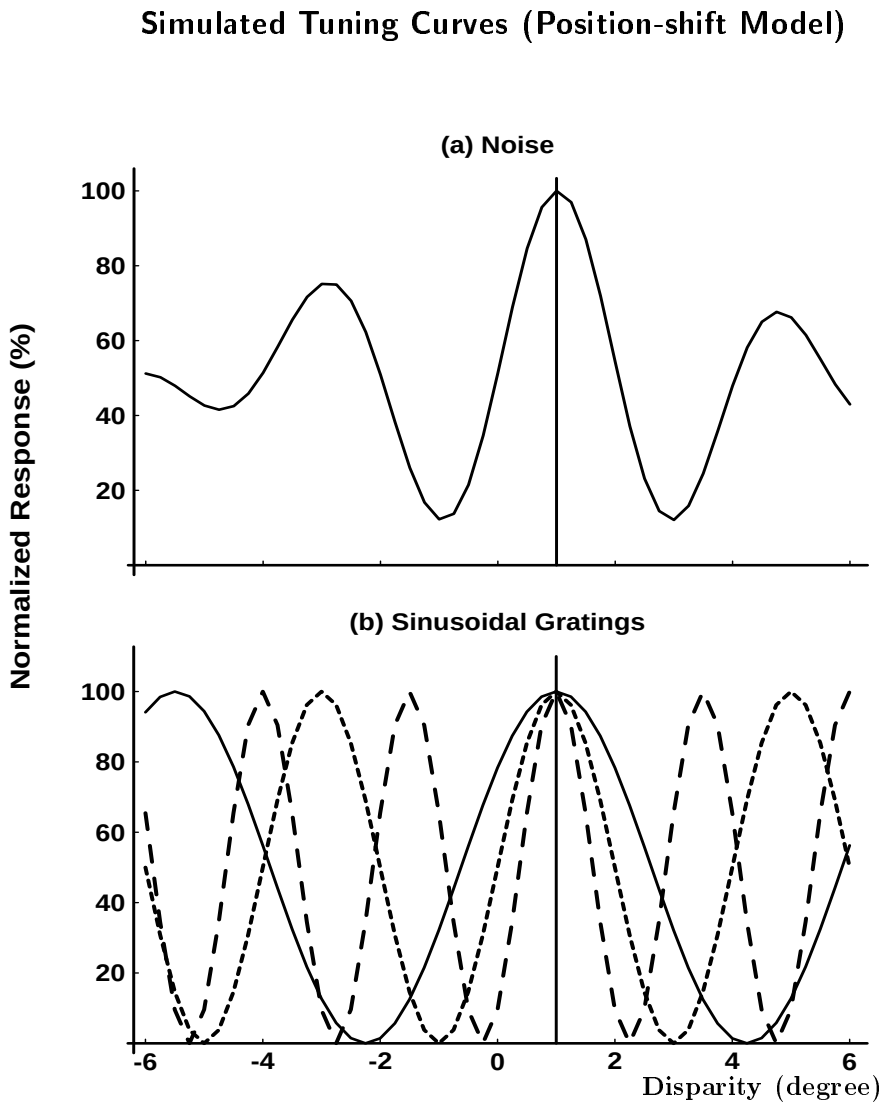

Fig.5 Zhu & Qian

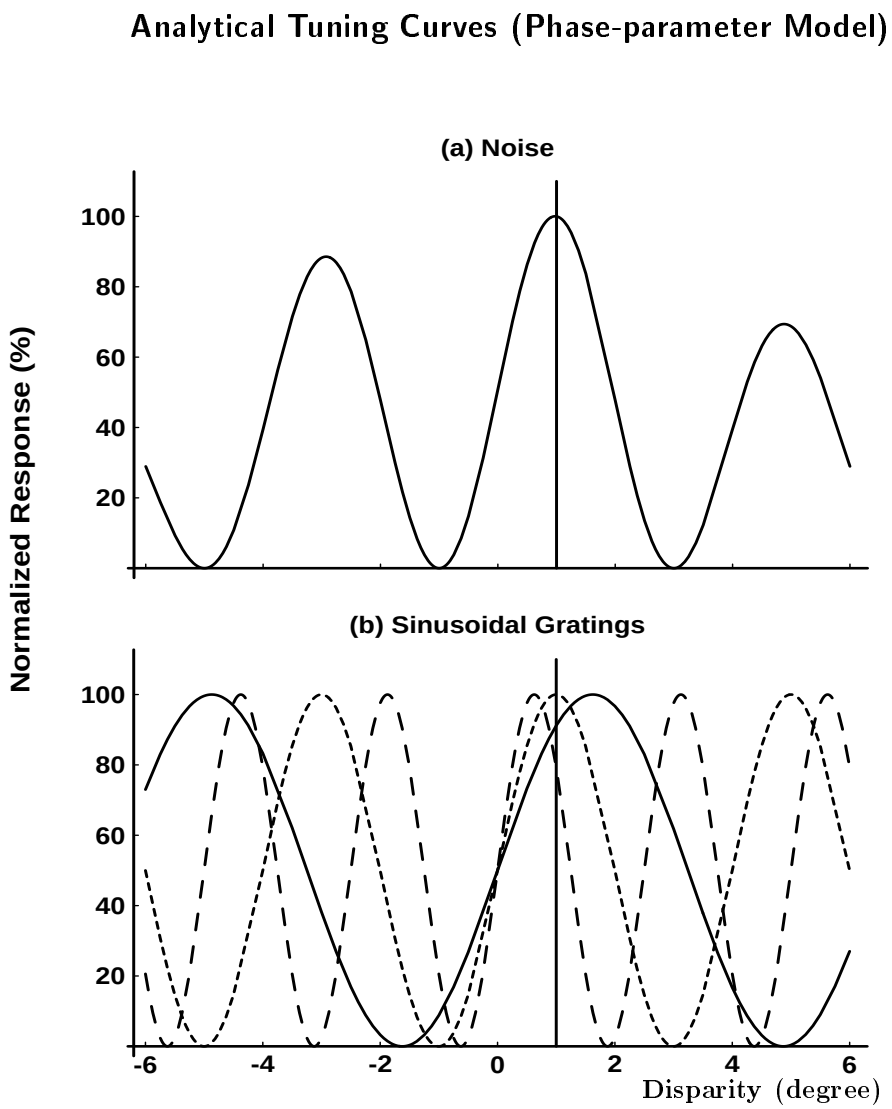

Fig.6 Zhu & Qian

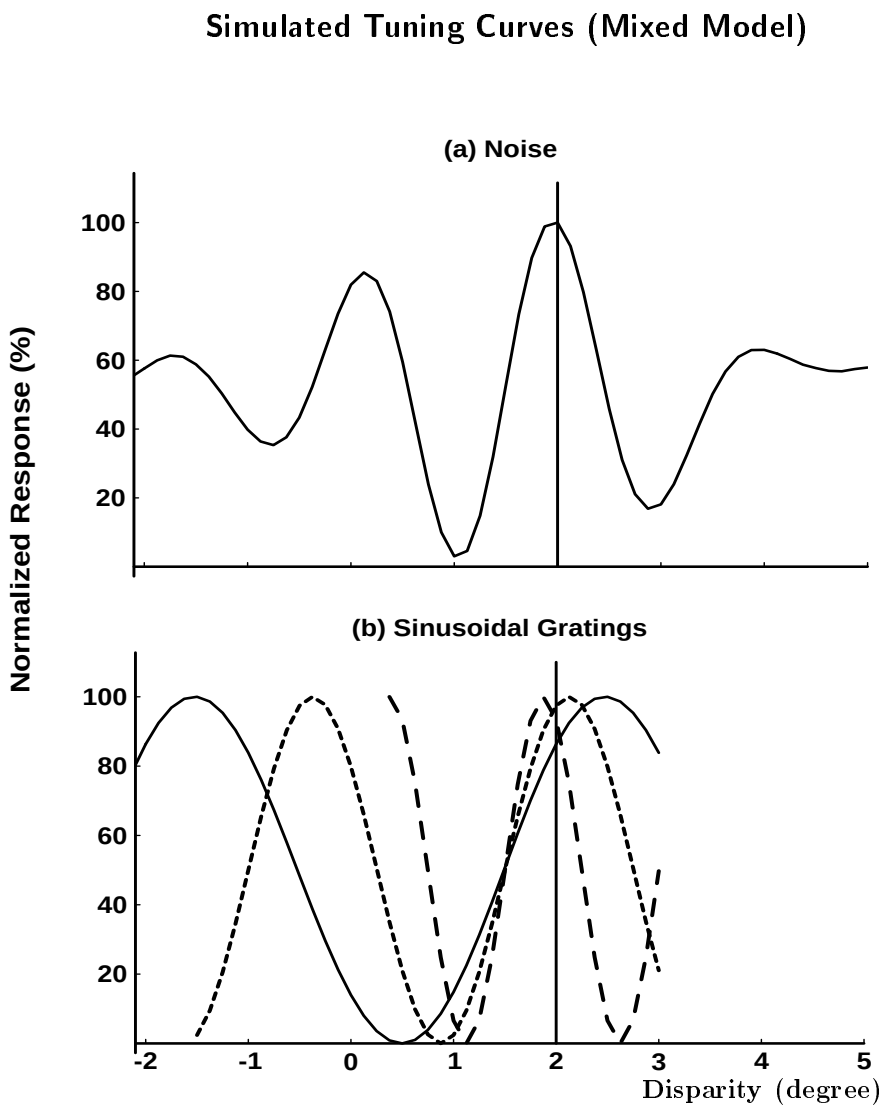

Fig.8 Zhu & Qian